Cell cycle regulation of oscillations yields coupling of growth and form in a computational model of the presomitic mesoderm

Murray, P. J.; Carrieri, F. A.; Dale, J. K.

Published in:
Journal of Theoretical Biology

DOI:
10.1016/j.jtbi.2019.05.006

Publication date:
2019

Cell cycle regulation of oscillations yields coupling of growth and form in a computational model of the presomitic mesoderm

Murray, P.J.[1], Carrieri, F. A.[2], and Dale, J. K.[2]

[1]Department of Mathematics, University of Dundee, Nethergate, Dundee, DD14HN, Scotland, UK.
[2]Division of Cell and Developmental Biology, School of Life Sciences, University of Dundee, Dow Street, Dundee, DD15EH, Scotland, UK.

Abstract

A striking example of coupling between growth and form occurs during the segmentation of the vertebrate embryo. During segmentation, pairs of segments, one on either side of the anterior-posterior axis, bud off from the presomitic mesoderm (PSM) at regular intervals in time. In the clock and wavefront model, a multicellular oscillator regulates the time at which the next pair of segments form whilst a wavefront regulates their spatial location. In most mathematical models of segmentation, it is assumed that cells in the PSM are oscillators with a constant characteristic frequency. Based on recent experimental findings, here we propose a model in which the natural oscillation frequency of each PSM cell is a function of its position in the cell cycle. Given adequate oscillator coupling and that cells in the PSM are randomly distributed in the cell cycle, we find that the emergent oscillator period is a weighted average of the constituent oscillator frequencies with the weightings dependent on the fraction of cells in a given cell cycle state. Here, we show that such a model can allow for coupling between pattern formation and growth rate in PSM tissue.

1 Introduction

The development of an embryo is a remarkably reproducible and robust process. Whilst our knowledge of the molecular pathways underpinning development has increased dramatically, many principles underpinning how growth of the embryo is coupled to form remain undiscovered.

A particularly striking example of pattern robustness arises during somitogenesis of the vertebrate embryo. Here, the trunk of the embryo segments at species-specific, regular intervals in time in a highly reproducible manner (Gibb

et al., 2010; Pourquié, 2018). Within each individual embryo, there is a remarkably stereotyped pattern of segments. Moreover, scaling phenomena, whereby the somite size varies as a function of PSM size, have been observed in multiple species (Cooke, 1975; Lauschke et al., 2013; Ishimatsu et al., 2018).

Whilst the formation of each pair of segments is preceded by a wave of anteriorly travelling oscillatory gene expression, it is not fully understood precisely how the dynamic patterns of clock gene expression affect segment size. In the clock and wave front model of somite formation (Cooke and Zeeman, 1976), an oscillator that resides in the PSM regulates the time at which the next segment boundary forms whilst a wavefront that sits in the posteriorly moving tail specifies the position of the next segment boundary. Owing to the discovery of a molecular oscillator, known as the segmentation clock, and gradients in multiple vertebrate species, the clock and wavefront model has gained significant traction.

The segmentation clock is comprised of a population of coupled genetic oscillators (Delaune et al., 2012; Lauschke et al., 2013; Masamizu et al., 2006; Soroldoni et al., 2014) that depend on numerous molecular pathways (e.g. Fgf, Wnt, Notch (Dequéant et al., 2006; Krol et al., 2011; Hubaud and Pourquié, 2014)). Notch signalling plays a fundamental role in the emergence of synchronous, tissue scale oscillations (Jiang et al., 2000; Ferjentsik et al., 2009; Okubo et al., 2012). In canonical Notch signalling, a Delta ligand in one cell binds to a Notch receptor in another, eventually resulting in the release of the Notch Intracellular Domain (NICD) (Hori et al., 2013; D'Souza et al., 2010). NICD translocates to the nucleus and forms a transcription complex that activates the transcription of Hes/Her genes, which are key negative regulators of the somitogenesis clock.

Recent *in vivo* work in both mouse and chick PSM tissue has shown that embryo treatment with a particular class of pharmacological perturbations results in an increased NICD half-life, higher levels of NICD, a longer clock period and larger segments (Wiedermann et al., 2015). In a follow-up study in *in vitro* cell lines, it has been shown that the cyclin dependent kinases CDK1 and CDK2 are molecular targets of the aforementioned pharmacological perturbations and that CDK1 and CDK2-mediated phosphorylation of NICD results in an increased rate of degradation (Carrieri et al., 2019). Moreover, the study showed that levels of NICD in *in vitro* cell lines fluctuate in a cell cycle dependent manner with lower levels seen in cell cycle phases in which CDK1 or CDK2 activity are high. Inhibiting CDK activity in mouse PSM tissue resulted in a similar phenotype to that observed by Wiedermann et al. (2015), i.e. higher levels of NICD and a longer clock period. A consistent interpretation of these data is that as CDK activity levels in PSM cells vary through the cell cycle, so the phosphorylation status of NICD and hence its degradation rate also varies. As we have found that higher levels of NICD are correlated with a longer clock period, we proposed the hypothesis that the natural oscillation frequency of an individual cell is modulated by position in the cell cycle (Carrieri et al., 2019).

Notably, the cell cycle has previously been shown to affect segmentation of the vertebrate embryo. Prior to the discovery of molecular clock and wavefronts in the PSM, Stern and colleagues (Primmett et al., 1988, 1989) performed a series of experiments in the chick embryo in which heat shock and a variety of chemical perturbations to the cell cycle exhibited a phenotype in which somite aberrations

were observed at intervals of approximately six somites. As the time taken to generate six somites in the chick embryo is approximately equal to the cell cycle duration, the authors proposed a cell cycle model of somitogenesis in which cells that entered the PSM together differentiated together. Subsequently, this model was formulated using a system of partial differential equations (Collier et al., 2000). Further evidence for cell cycle coupling to the somitogenesis clock has been found in the zebrafish where during M phase of the cell cycle it has been shown that a cell's segmentation clock oscillator pauses, resulting in its oscillator phase lagging that of the tissue upon reentry into the cell cycle (Horikawa et al., 2006). Whilst coupling from the segmentation clock to the cell cycle has been less well studied, in the zebrafish embryo it has been observed that mitosis preferentially occurs in the off phase of the segmentation clock cycle (Delaune et al., 2012).

In this study, we explore a computational model of the PSM in which there is a heterogeneous distribution of cell cycle dependent oscillation frequencies. The model is used to demonstrate *in silico* the hypothesis that cell cycle coupling to the segmentation clock can buffer pattern wavelength from the effect of global perturbations to the PSM growth rate. The layout is as follows: in Section 2 we present a computational model of cell cycle-coupled oscillations in the PSM; in Section 3 we introduce a minimal model of coupled, cell cycle-dependent oscillators and show that the emergent oscillator period can be tuned by the cell cycle distribution. We then consider the behaviour of constant and cell cycle dependent-frequency models of PSM oscillations in the context of a clock and wavefront model and test the hypothesis that cell cycle-coupled PSM oscillations can be robust to variation in embryo growth rate. Finally, in Section 4 we conclude with a discussion.

2 Methods

Model Development

To describe the progression of individual cells through the somitogenesis clock cycle, we consider a phase coupled oscillator model given by

$$\frac{d\theta_i}{dt} = \omega_i(C_i(t)) + A\sum_j \sin(\theta_j - \theta_i), \quad i = 1, .., N, \tag{1}$$

where $\theta_i(t)$ represents the phase of the i^{th} cell at time t, ω_i represents the natural frequency of the i^{th} cell at time t, $C_i(t)$ represents the position of the i^{th} cell in the cell cycle at time t, the sum is taken over nearest neighbours and A is a coupling strength. Nearest neighbours are defined using a cut-off rule: cells that are positioned within a distance δ of the i^{th} cell are defined to be its neighbours.

The variable $C_i(t)$, a measure of cell cycle progression, tracks the time that has elapsed since the last cell division. Hence

$$\frac{dC_i}{dt} = 1,$$

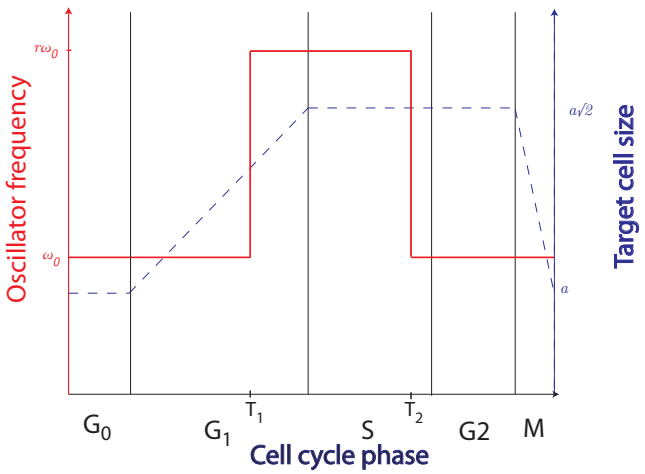

Figure 1: A schematic illustration of a model for cell cycle modulated oscillator frequency. Oscillator frequency (solid red line) and cell target size (dashed blue line) are plotted against cell cycle phase. Vertical lines delineate cell cycle phases.

with cell cycle phase, P_i, defined as follows:

$$P_i = \begin{cases} G_0 & C_i \in [0, T_{G_0}], \\ G_1 & C_i \in [T_{G_0}, T_{G_0} + T_{G_1}], \\ S & C_i \in [T_{G_0} + T_{G_1}, T_{G_0} + T_{G_1} + T_S], \\ G_2 & C_i \in [T_{G_0} + T_{G_1} + T_S, T_{G_0} + T_{G_1} + T_S + T_{G_2}], \\ M & C_i \in [T_{G_0} + T_{G_1} + T_S + T_{G_2}, T_{G_0} + T_{G_1} + T_S + T_{G_2} + T_M], \end{cases} \tag{2}$$

where T_{G_0}, T_{G_1}, T_S, T_{G_2} and T_M represent the durations of G_0, G_1, T_S, G_2 and M (see Table 1 for parameter values).

In this study, following experimental work by Wiedermann et al. (2015) and Carrieri et al. (2019), it is assumed that the cell cycle modulates a cell's natural oscillator frequency (see Figure 1). Although Carrieri et al. (2019) have identified that both CDK2 and CDK1 can modify NICD stability at the $G_1 - S$ and $G_2 - M$ transitions, respectively, here, for the sake of model simplicity, we assume an effect only at the $G_1 - S$ transition. The key model assumption is that a cell's natural oscillator frequency, ω_0, increases by a factor r at the $G_1 - S$ transition, i.e.

$$\omega_i(C) = \begin{cases} r\omega_0 & C_i \in [T_1, T_2], \\ \omega_0 & \text{otherwise}, \end{cases} \tag{3}$$

where T_1 and T_2 define the interval during which the oscillation rate is increased.

Note that in Section 3 the consequences of cell cycle coupling to the somitogenesis oscillator will be explored. The null (constant oscillator frequency) model, where there is no coupling to the cell cycle, is captured by setting $r = 1$ as the oscillator frequency is ω_0 throughout the cell cycle. For cell cycle dependence, $r > 1$.

Assuming that cell growth occurs during G_1 phase of the cell cycle, here we suppose that the cell radius increases linearly in time throughout G_1 of the cell

cycle so that the cell area approximately doubles, i.e.

$$a(C_i) = \begin{cases} G_0 & \tilde{a}, \\ G_1 & \tilde{a}\left(1 + (\sqrt{2}-1)\frac{C_i - T_{G_0}}{T_{G_1}}\right), \\ S & \tilde{a}\sqrt{2}, \\ G_2 & \tilde{a}\sqrt{2}, \\ M & \tilde{a}, \end{cases} \tag{4}$$

where $\tilde{a}$ is the cell radius after division. When the cell cycle of the i^{th} reaches the end of the cell cycle, C_i is reset such that $C_i = 0$, the cell divides, randomly samples G_1 and G_2 durations and places a daughter cell adjacent to it in a randomly chosen direction.

To describe cell mechanics in the PSM, we let $\mathbf{r}_i(t)$ represent the spatial position of the i^{th} cell in a model of the PSM defined in two spatial dimensions. It is assumed that motion is over-damped and that cells interact via an intercellular force law, F, i.e.

$$\frac{d\mathbf{r}_i}{dt} = \sum_j \mathbf{F}(\mathbf{r}_i - \mathbf{r}_j). \tag{5}$$

where the sum is taken over nearest neighbours. Defining the equilibrium separation distance between the i^{th} and j^{th} cells, i.e. an effective resting spring length, to be

$$a_{ij} = a(C_i) + a(C_j),$$

the overlap is defined to be

$$r_{ij} = |\mathbf{r}_i - \mathbf{r}_j| - a_{ij}.$$

For overlapping cells (i.e. $r_{ij} < 0$), the elastic force between two cells is given by

$$\mathbf{F} = k a_{ij} \ln\left(1 + \frac{r_{ij}}{a_{ij}}\right) \frac{(\mathbf{r}_i - \mathbf{r}_j)}{|(\mathbf{r}_i - \mathbf{r}_j)|}, \tag{6}$$

where k is a spring constant (Fletcher, 2010).

A minimal clock and wavefront model

To consider the effect of cell cycle -coupled PSM oscillators on pattern formation in the PSM, we consider a cell-based model in which cells are confined to reside in a semi-infinite domain of width L_x. Each cell in the PSM can grow, progress through the cell cycle and divide. Additionally, each cell in the PSM has a somitogenesis clock that is coupled to its nearest neighbours. $L_P(t)$ is defined to be the position of the posterior boundary of the PSM and it is assumed that oscillations occur only in the region $y \in [L_p(t) - L_y, L_p(t)]$, where the constant L_y is defined to be the length of the oscillatory region of the PSM. When the i^{th} cell crosses the boundary $y = L_p(t) - L_y$ (see Figure 2) at some time t_i^*, it stops oscillating and its phase is fixed in time, i.e.

$$\theta_i(t) = \theta_i(t_i^*), \quad t > t_i^*.$$

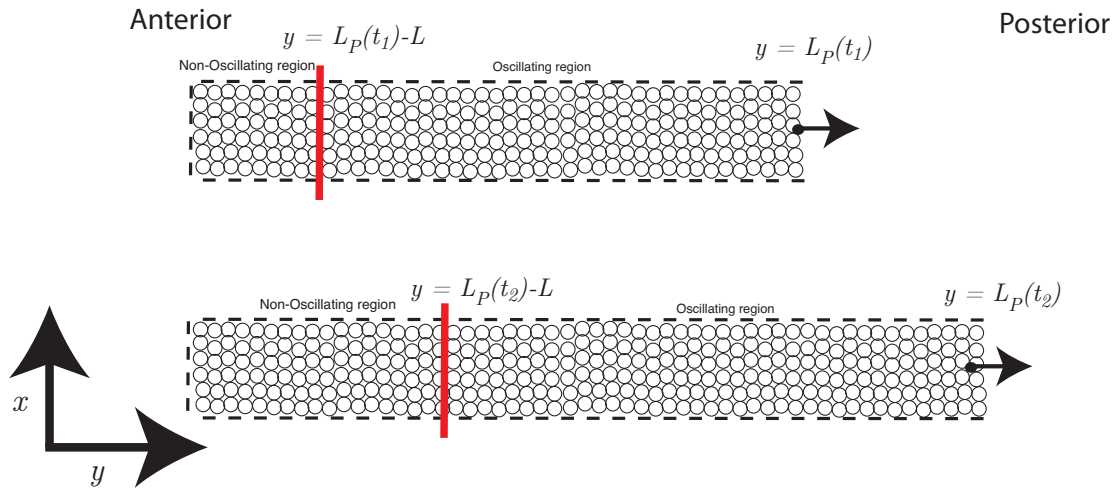

Figure 2: A schematic illustration of the model of the PSM at times $t = t_1$ (left) and $t = t_2$ (right, $t_2 > t_1$). The oscillating region is defined such that $y \in [L_p(t) - L_y, L_p(t)]$ where $L_p(t)$ denotes the posterior boundary of the PSM at time t (black dot), $L_p(t) - L_y$ denotes the anterior boundary of the PSM (red line) and L_y is the length of the oscillating region. Dashed lines denote hard boundaries.

The above conditions yields an integral form of the clock and wavefront result $S = vT$. Suppose the last boundary formed at position S_{k-1} and time t_{k-1}. The position of the next boundary will occur at position

$$S_k = S_{k-1} + \int_{t_{k-1}}^{t_k} v(t)dt,$$

where $v(t)$ represents the velocity of the wavefront and t_k satisfies

$$\int_{t_{k-1}}^{t_k} \omega(t)dt = 2\pi$$

Note that in the case of constant oscillator frequency and wavefront velocity

$$S = vT.$$

Hard wall boundary conditions are given by

$$\frac{d\mathbf{r}_i}{dt} \cdot \mathbf{n} = 0$$

and imposed on the lines $x = 0$, $x = L_x$ and $y = 0$ (normals are $\mathbf{n} = [-1, 0]$, $\mathbf{n} = [1, 0]$ and $\mathbf{n} = [0, -1]$, respectively).

Simulations

Equations (1)- (4) were implemented using the Chaste software environment (Pitt-Francis et al., 2009). Parameter values are presented in Table 1. The initial

Parameter	Value	Unit	Description	Reference
ω_0	1.39	h^{-1}	somitogenesis clock frequency	
A	50.0	h^{-1}	oscillator coupling strength	
r	4.5	Dimensionless	somitogenesis clock acceleration factor	
T_{G_0}	0.0	h	G_0 duration	
T_{G_1}	$3.0+E_{[3]}$	h	G_1 duration	
T_S	3.0	h	S duration	
T_{G_2}	$2.0+E_{[3]}$	h	G_2 duration	
T_M	1	h	M duration	
T_1	$T_{G_0} + T_{G_1} - 2.0$	h	Start of clock acceleration	
T_2	$T_{G_0} + T_{G_1} + T_S - 1.0$	h	End of clock acceleration	
k	400	h^{-1}	spring constant	
$\tilde{a}$	0.375	non dim	cell radius after division	
t^*	65.0	h	time at which G_0 is half maximal	
C	4.5	h	maximal G_0	
L_x	5.0	c.d.	PSM width	
L_y	35.0	c.d.	PSM length	
δ	1.5	c.d.	nearest neighbour cut-off threshold	
dt	0.001	h	time step	
τ	4.0	h	G_0 increase time scale	

Table 1: A table with parameter values. $E_{[z]}$ denotes random variable sampled from an exponential distribution with mean z.

conditions are chosen such that at $t = 0$ a 5×20 honeycomb mesh of cells are initially uniformly distributed in the cell cycle, i.e.

$$C_i = U_{[0,T_C]}$$

To avoid artefacts from the initial data, the cell population is simulated in the interval $t \in [0, 50\ ]$ h. At $t = 50$ h, the somitogenesis clock model is initialised with spatially homogeneous initial conditions

$$\theta_i = 0, \qquad \forall i$$

and the model is simulated in the interval $t \in [50, 100\ ]$h.

Metrics

Global order of the cell population is computed using

$$\rho(t)e^{i\Psi(t)} = \frac{1}{N}\sum_{j=1}^{N} e^{i\theta_j(t)}, \tag{7}$$

where $i = \sqrt{-1}$, N is the number of oscillators in the PSM and $\rho(t)$ and $\Psi(t)$ represent the order parameter and the average phase at time, t, respectively. The average frequency of the PSM is computed to be

$$\Omega(t) = \frac{1}{N}\sum_{j=1}^{N} \frac{d\theta_j}{dt}.$$

The pattern wavelength, S, is computed by plotting $\sin(\theta_j)$ against y_j for every cell in the PSM. The peaks of the distribution are identified using the Matlab command 'findpeaks'. Suppose consecutive peaks are identified at position y_k and y_{k+1}. The length of the k^{th} segment is defined to be

$$S_k(y^*) = y_{k+1} - y_k,$$

where

$$y^* = \frac{y_k + y_{k+1}}{2}.$$

3 Results

3.1 Cell cycle coupling can tune the emergent frequency of PSM oscillators

To investigate the effect of cell cycle coupling on the emergent frequency, equations (1)-(3) were solved on a fixed regular hexagonal lattice in which cells had a model for cell cycle dynamics but did not divide (see Supplementary Movie 1). In the case where $r > 1$ (i.e. cell cycle coupling to the clock frequency), we found that: (i) the emergent oscillator frequency, Ω, was largely independent of the coupling strength A (see Figure 3 (a)); and (ii) for large enough values of coupling strength, A,

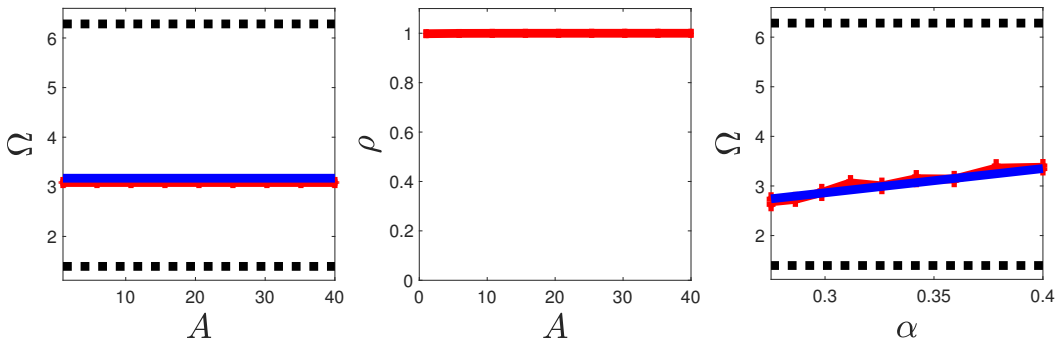

(a) (b) (c)

Figure 3: Emergent oscillator frequency in a cell-cycle modulated natural oscillator frequency model. (a) The average oscillator frequency, Ω, is plotted against oscillator coupling strength, A. Red line - simulation. Blue line - equation (8). Dotted lines - minimal (ω_0) and maximal frequencies ($r\omega_0$). (b) The order parameter, ρ, is plotted against oscillator coupling strength, A (see equation (7)). (c) The average oscillator frequency, Ω, is plotted as a function of α, the fraction of the cell cycle in which cells oscillate with a higher frequency. Solid blue line - simulation. Dashed red line - equation (8). Dotted lines - minimal (ω_0) and maximal frequencies ($r\omega_0$).

oscillator coupling can synchronise the population (see Figure 3 (b)). Additionally, the emergent oscillator frequency is a weighted average of the constituent oscillator frequencies (see Figure 3 (c)).

Assuming that oscillator coupling is strong enough to synchronise the oscillators in the PSM, we find that the emergent average frequency of the population can be estimated as a weighted-average of the individual oscillation frequencies, i.e.

$$\Omega = \omega_0 \left(1 - \alpha + r\alpha\right), \tag{8}$$

where

$$\alpha = \frac{T_2 - T_1}{T_{CC}}, \tag{9}$$

and $T_{CC} = T_{G_0} + T_{G_1} + T_S + T_{G_2} + T_M$. These results show that a cell cycle-coupled two-frequency model of the somitogenesis oscillator yields an emergent frequency that can be tuned by the distribution of cells within the cell cycle.

3.2 Constant growth patterns

To explore whether a population of oscillator frequencies can result in robust pattern formation in an *in silico* model of segment patterning, a minimal clock and wavefront model was constructed (as described in Section 2).

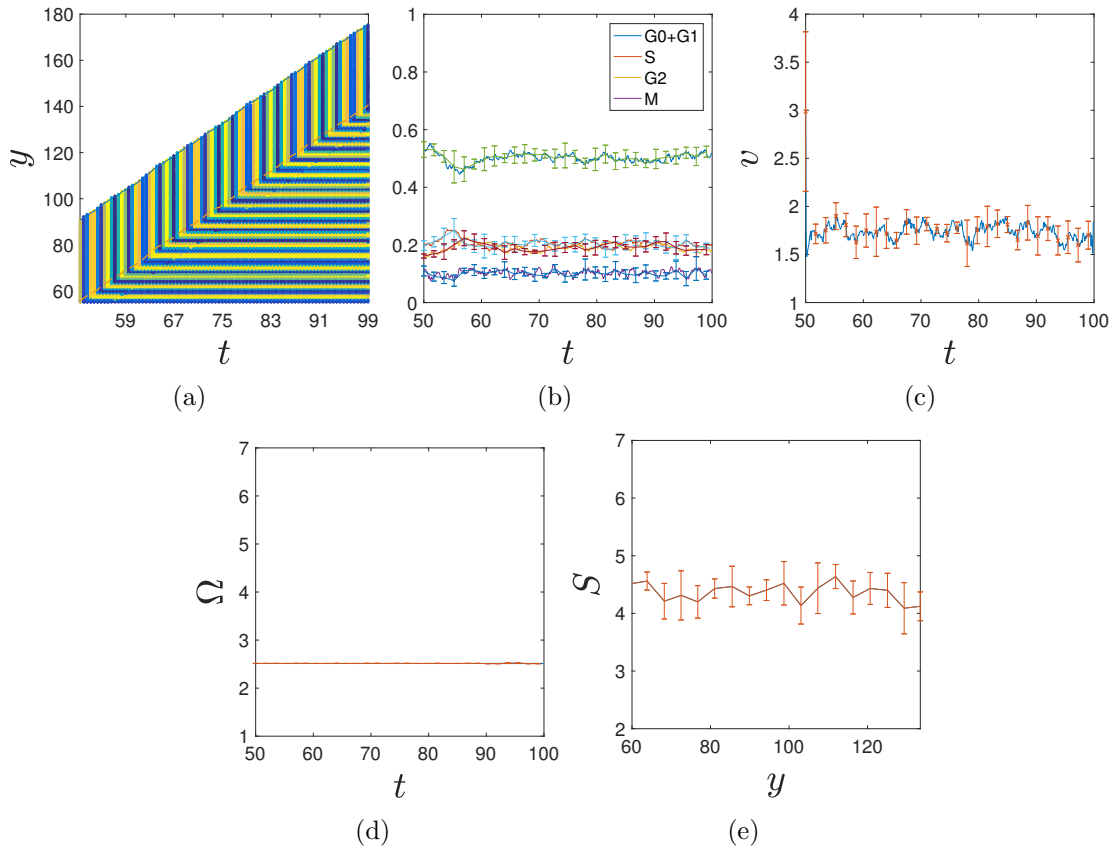

Figure 4: Constant pattern wavelength in a clock and wavefront model. (a) Phase dynamics plotted against space and time, t, in a representative simulation. (b) The proportion of cells in different cell cycle phases is plotted against time, t. (c) The velocity of the posterior tip of the PSM, v_P, is plotted against time, t. (d) The emergent tissue oscillation rate, Ω, in the posterior PSM is plotted against time, t. (e) The steady state pattern wavelength, S, is plotted against axial position, y. Equations (1) - (4) were solve as described in Section 2. $r = 1$. Other parameter values as in Table 1.

Pattern formation in the null model yields constant pattern wavelength

To verify that the null model (equations (1) - (4), $r = 1$) introduced in Section 2 yields expected results, in Figure 4 (a) we present phase dynamics from a representative simulation (see Supplementary Movie 2). Note that the distribution of cells in the cell cycle is approximately constant (Figure 4 (b)) and that the PSM grows at an approximately constant rate (Figure 4 (c)). As each cell has a fixed oscillator frequency, the tissue averaged oscillator frequency is constant (Figure 4 (d)). The proposed clock and wavefront mechanism yields a pattern wavelength of approximately constant size (Figure 4 (e)).

An emergent oscillator frequency in a two frequency, cell cycle-coupled model of the posterior PSM

To explore whether the introduction of cell cycle dependence on oscillator frequency yields robust pattern formation in an *in silico* model of segment patterning, we adapted the null model so that a PSM cell's natural oscillator frequency is a function of the cell cycle (equations (1) - (4), $r = 4.5$, see Supplementary Movie 3).

We found that, as expected, sufficiently strong oscillator coupling is required for synchronisation of a system with a heterogeneous distribution of natural oscillator frequencies (results not shown). In Figure 5 (a) we depict numerical simulations from the cell cycle-coupled model. As expected, the cell cycle dynamics and posterior tip velocities (Figure 4 (b) and (c), respectively) show similar profiles to the corresponding plots in Figure 4. However, as a result of cell cycle coupling, the tissue averaged oscillator frequency, $\Omega(t)$, varies in time (see Figure 5 (b)-(d)). The resulting pattern wavelength is approximately constant along the axis (see Figure 5 (e)). A key feature of the model is that, similar to the results presented in Figure 3, the emergent oscillation rate, $\Omega(t)$, can be approximated as being a weighted average of the constituent oscillator frequencies. Hence, in the proposed model, the pattern wavelength can be tuned via modulation of the cell cycle.

3.3 Global growth patterns

To test the hypothesis that cell cycle coupling can couple growth and form in a clock and wavefront model of pattern formation in the PSM, an increase in cell cycle duration is imposed via the equation

$$T_{G_0} = \frac{C}{2}\left(1 + \tanh\left(\frac{(t - t^*)}{\tau}\right)\right), \tag{10}$$

where t^* is the time at which T_{G_0} is half maximal, C is the maximal increase in G_0 duration and τ defines the time scale over which G_0 increases. Hence, early in the simulation T_{G_0} is approximately 0 but it increases to a maximal value C. Biologically, this could represent a delay in a cell reentering the cell cycle at the end of M phase.

Variable pattern wavelength upon growth perturbation in a constant frequency model

We first consider the behaviour of the null model (equations (1) - (4), $r = 1$) together with the growth condition given by equation (10) (see Supplementary Movie 4). Figure 6 (a) depicts phase dynamics similar to the constant growth rate case (see Figure 4) with regular synchronised oscillations in the posterior PSM. As time evolves, the fraction of cells in G_0 increases (Figure 6 (b)) and the posterior tip velocity, $v_P(t)$, decreases (Figure 6 (c)). As the somitogenesis clock frequency is constant (Figure 6 (d)), the effect of the reduced posterior tip velocity is to reduce pattern wavelength (Figure 6 (e)). Hence, in the proposed model pattern wavelength is not robust to slow perturbation to the tissue growth rate.

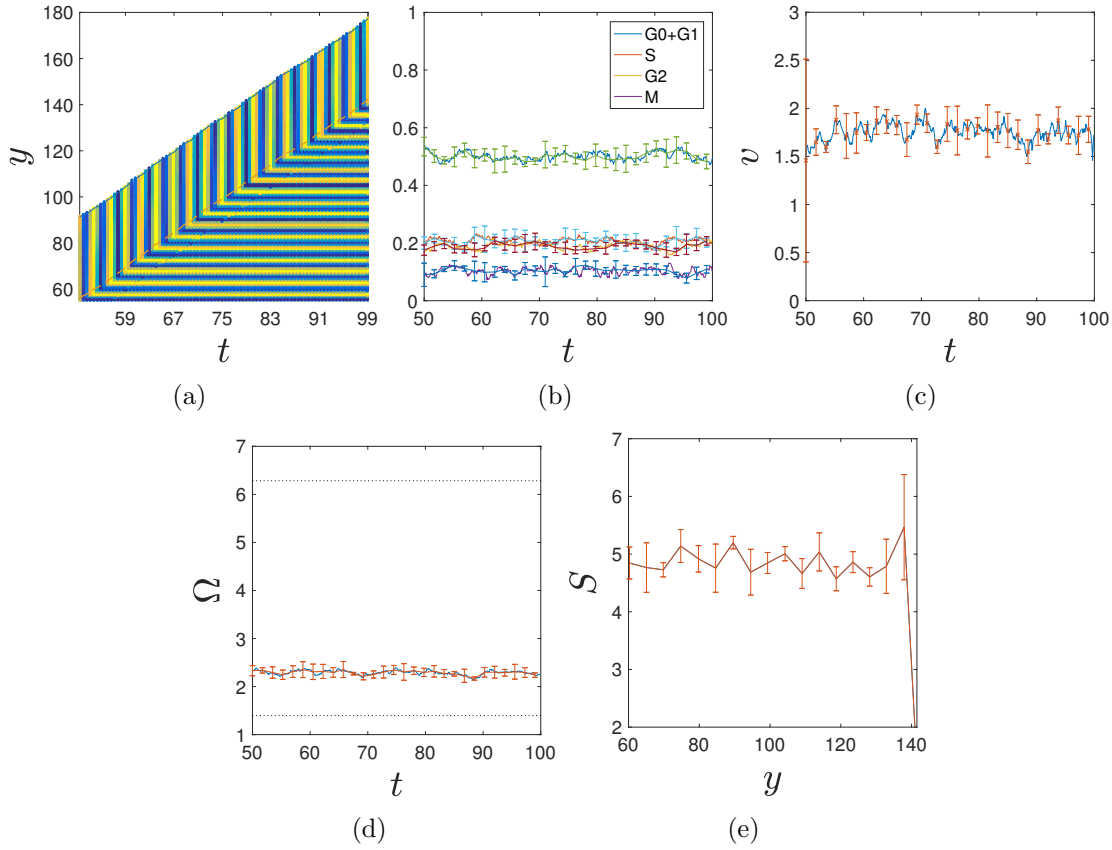

Figure 5: Constant pattern wavelength in a cell cycle coupled clock and wavefront model. (a) Phase dynamics plotted against space, y, and time, t. (b) The proportion of cells in different cell cycle phases is plotted against time, t. (c) The velocity of the posterior tip of the PSM, v_P, is plotted against time, t. (d) The average tissue oscillation rate, Ω, in the posterior PSM is plotted against time, t. Dotted lines - minimal (ω_0) and maximal frequencies ($r\omega_0$). (e) The steady state pattern wavelength, S, is plotted against axial position, y. Equations (1) - (4) were solve as described in Section 2. Other parameter values as in Table 1.

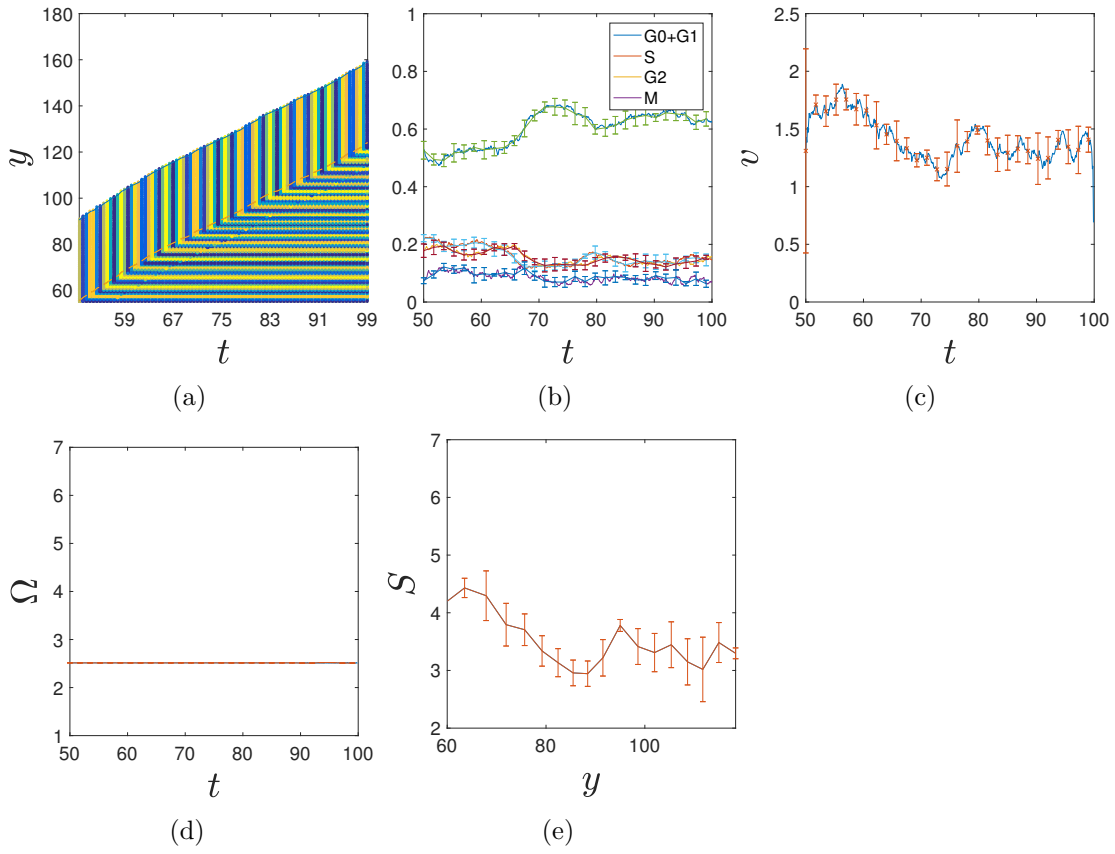

Figure 6: Decreasing pattern wavelength in a clock and wavefront model with non-uniform growth. (a) Phase dynamics plotted against space and time. (b) The proportion of cells in different cell cycle phases is plotted against time, t. (c) The velocity of the posterior tip of the PSM, v_P, is plotted against time, t. (d) The average tissue oscillation rate, Ω, in the posterior PSM is plotted against time, t. (e) The steady state pattern wavelength, S, is plotted against axial position, y. Equations (1) - (4) and (10) were solve as described in Section 2. $r = 1$. Other parameter values as in Table 1.

Cell cycle coupling can compensate for global patterning of tissue growth

To investigate whether cell cycle coupling to the somitogenesis clock can in principle make pattern formation robust to the presence of perturbation in the growth dynamics of the PSM, the cell cycle-coupled oscillator frequency model (equations (1) - (4), $r = 4.5$) was simulated in the case of global variation in the tissue growth rate defined by equation (10) (see Figure 7 (a) for phase dynamics in a representative simulation and Supplementary Movie 5). As is the case in Figure 6, as a result of the imposed increase in G_0 time given by equation (10), the fraction of cells in G_0 increases in time and the posterior tip velocity, $v_P(t)$, decreases (Figure 7 (b) and (c), respectively). For this model, the effect of cell cycle coupling to the tissue averaged oscillation frequency is that the decreasing tissue growth rate is coupled with a decreasing averaged tissue oscillation rate (Figure 7 (d)). The trend of decreasing pattern wavelength observed in Figure 6 is reduced (see Figure 7 (e)). These simulation results show that coupling emergent tissue scale oscillation frequency to the tissue scale growth rate can result in a buffering of the final pattern to variation in the growth rate. Hence, in the proposed model the pattern wavelength is coupled to the the tissue growth rate.

4 Conclusions

The coupling of growth and form is a necessity for many patterning processes that arise during embryo development. During somitogenesis, pairs of segments form at regular intervals in space and time with a temporal periodicity that is regulated by a population of coupled oscillators that reside in the PSM.

Recent experimental work has suggested that the cell cycle modulates the natural oscillation frequency of cells in the PSM (Wiedermann et al., 2015; Carrieri et al., 2019). To investigate the consequences of this observation in the context of pattern formation in the PSM, we developed a cell cycle-dependent model of coupled oscillators in the PSM in which a PSM cell can have one of two natural frequencies. We show that in the presence of sufficiently strong oscillator coupling, the oscillators synchronise to an emergent frequency that is a weighted average of the constituent frequencies. Consequently, the emergent tissue period is a function of the distribution of cells in the cell cycle. Moreover, this model gives robust pattern formation when integrated into a cell-based implementation of the clock and wavefront model in PSM tissue.

To explore a possible role for cell cycle coupling to the segmentation clock, we consider a perturbation in which the cell cycle is extended by introducing a quiescent state in which a cell pauses its cell cycle after mitosis, resulting in a smaller PSM growth rate. The simulations show that the cell cycle coupled model exhibits a reduced effect on segment size as the emergent oscillator period increases.

In the clock and wavefront model of somitogenesis, the timing of boundary formation is regulated by a clock that resides in the PSM and the spatial location by a propagating wavefront. In contrast, motivated by experiments in the chick embryo show that perturbation of the cell cycle results in periodic defects in segmentation

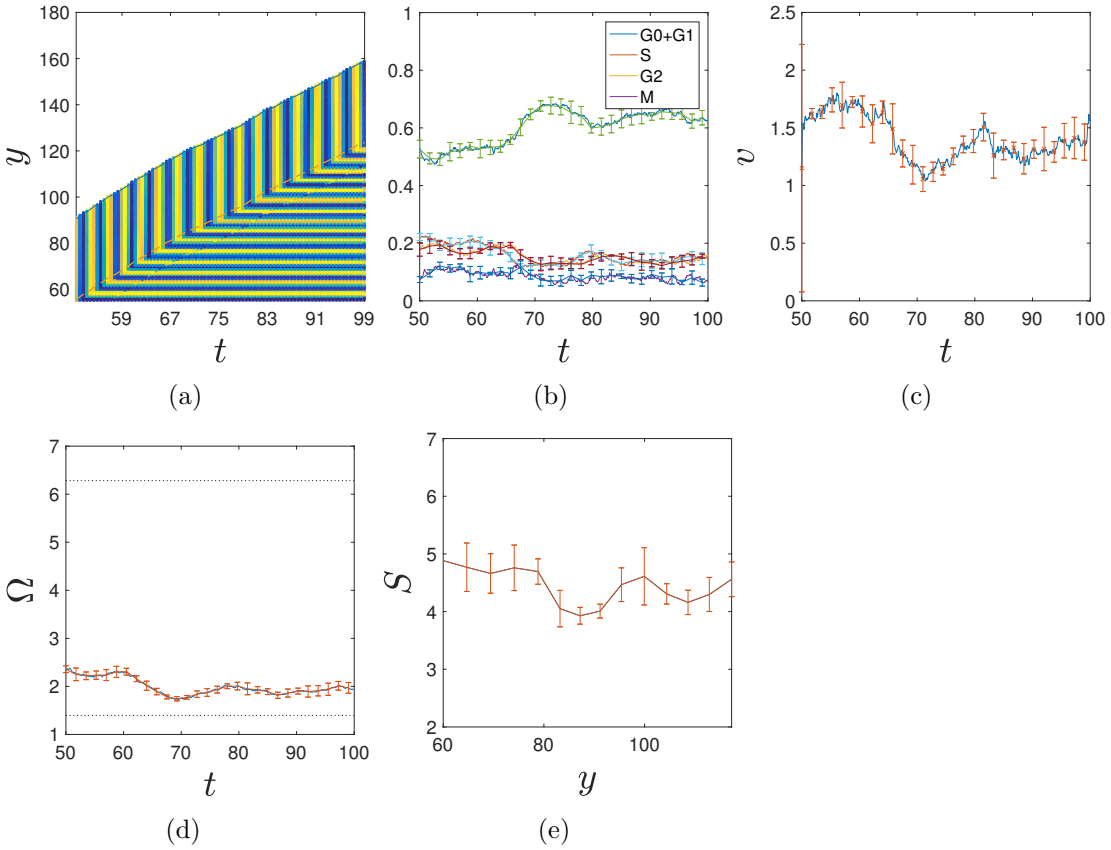

Figure 7: Compensated pattern wavelength in a clock and wavefront model with non-uniform growth and cell cycle coupling to PSM oscillations. (a) Phase dynamics plotted against space and time, t. (b) The proportion of cells in different cell cycle phases is plotted against time, t. (c) The velocity of the posterior tip of the PSM, v_P, is plotted against time, t. (d) The average tissue oscillation rate, Ω, in the posterior PSM is plotted against time, t. Dotted lines - minimal (ω_0) and maximal frequencies ($r\omega_0$). (e) The steady state pattern wavelength, S, is plotted against axial position, y. Equations (1) - (4) and (10) were solve as described in Section 2. Parameter values as in Table 1.

(Primmett et al., 1988, 1989). Whilst the discovery of the molecular components of a clock and a wavefront in numerous vertebrate species have led to the clock and a wavefront model being a widely accepted model of vertebrate segmentation, the experimental observations that motivated the cell cycle model have not, to the best of our knowledge, been explained within the context of a clock and wavefront model. We note that a feature of the proposed model is that perturbations to the equilibrium cell cycle distribution decay in an oscillatory manner with a period approximately equal to that of the cell cycle (see peaked profile in Figure 7). Hence the emergent oscillator period can exhibit oscillations on the time scale of the cell cycle. Whilst this feature of the model can potentially reconcile the cell cycle and clock and wavefront models of somitogenesis, further experiments are required in a system where the cell cycle distribution and somitogenesis clock period can be measured in tandem.

The major focus of this study is to explore principles of cell cycle coupling to the somitogenesis clock in individual cells. Whilst we have tried to use parameter values and dimensions that are broadly consistent with measurements from PSM tissue, the models are not species specific and we do not expect the results to quantitatively reproduce experimental observations. To the best of our knowledge, oscillator coupling strengths have not been directly estimated in PSM tissue; here we choose the value of the coupling strength to be large enough so as to guarantee that there is a spatially homogeneous phase distribution in the PSM. Furthermore, we have chosen the choice of the acceleration factor, r, to be large enough so as to observe an effect in the simulations. Future experiments are need to measure these parameters in a specifies-specific manner.

Whilst in this study we have considered the PSM to be a self-maintaining cell population, in the embryo cell movements resulting from gastrulation can result in a flux of cells into the the PSM. Whilst the proposed model does not account for such a flux, it could be tested experimentally in a tail culture system where PSM tails are cultured in vitro (e.g. Lauschke et al., 2013).

In the zebrafish it has been proposed that delayed coupling mediated by Notch signalling tunes the collective period of the segmentation clock (e.g. Morelli et al., 2009). In contrast, in this study we consider a model in which Notch signalling alters the individual period of single cells in a cell cycle dependent manner. This assumption is motivated by observations of correlation between NICD stability and the emergent somitogenesis clock period (Wiedermann et al., 2015) in the chick embryo. We note that further experiments are needed in order to measure in single cells whether there is a cell cycle dependent effect on the somitogenesis clock frequency.

The model explored in this study is minimal in the sense that modification to the clock frequency has been considered only at the G1-S transition of the cell cycle. Measurements from HEK293 cell lines (Carrieri et al., 2019) suggest a more complicated relationship than the one proposed in this study. In future work, we will seek to precisely measure the correlation between cell cycle state and clock frequency in PSM cells.

The major focus of this study was to explore the role of cell cycle regulation on emergent tissue period in the PSM. We note that the imposed model does not describe oscillatory waves observed *in vivo*, a phenomenon that has been described

by numerous approaches ((Murray et al., 2011, 2013; Morelli et al., 2009)). The main idea proposed in this study, that the distribution of cells in the cell cycle modulates the somitogenesis clock period, could be implemented in more detailed models of phase dynamics. Furthermore, to maintain as simple a description of the clock and wavefront mechanism as possible we have defined the wavefront to be a fixed distance from posterior tip of the PSM.

In a recent striking variant on the clock and wavefront model, known as the clock and scaled gradient model (Ishimatsu et al., 2018), the size of a forming segment depends on the PSM length four cycles ago. The model, supported by experiments in which surgical reduction in the PSM size results in a scaled segment size but an unchanged clock period, suggests that the clock period does not play a role in scaling phenomena. These experimental facts can be reconciled with the proposed two frequency model; as in the two frequency model the clock period is a function of the distribution of cells within the cell cycle, a surgical experiment that removes some of the PSM but does not change the distribution of cells within the cell cycle would not modify the clock period.

The major aim of this work was to explore *in silico* the behaviour of a two frequency, cell cycle-coupled model of the somitogenesis clock. The results show that a potential role, consistent with existing experimental evidence, could be to couple the rate of tissue growth to pattern wavelength such that slower growing PSM does not necessarily yield smaller segments. To further refine and validate the proposed model, a set of experiments is required that precisely measures coupling between the cell cycle and the somitogenesis clock in both uncoupled PSM cells and in tissue contexts.

References

F. A. Carrieri, P. J. Murray, D. Ditsova, M. A. Ferris, P. Davies, and J. K. Dale. CDK1 and CDK2 regulate NICD turnover and the periodicity of the segmentation clock. *EMBO reports*, page e46436, 2019.

J. R. Collier, D. McInerney, S. Schnell, P. K. Maini, D. J. Gavaghan, P. Houston, and C. D. Stern. A cell cycle model for somitogenesis: mathematical formulation and numerical simulation. *Journal of Theoretical Biology*, 207(3):305–316, 2000.

J. Cooke. Control of somite number during morphogenesis of a vertebrate, xenopus laevis. *Nature*, 254(5497):196, 1975.

J. Cooke and E. C. Zeeman. A clock and wavefront model for control of the number of repeated structures during animal morphogenesis. *Journal of Theoretical Biology*, 58(2):455–476, 1976.

E. A. Delaune, P. François, N. P. Shih, and S. L. Amacher. Single-cell-resolution imaging of the impact of notch signaling and mitosis on segmentation clock dynamics. *Developmental Cell*, 23(5):995–1005, 2012.

M.-L. Dequéant, E. Glynn, K. Gaudenz, M. Wahl, J. Chen, A. Mushegian, and O. Pourquié. A complex oscillating network of signaling genes underlies the mouse segmentation clock. *Science*, 314(5805):1595–1598, 2006.

B. D'Souza, L. Meloty-Kapella, and G. Weinmaster. Canonical and non-canonical notch ligands. *Current Topics in Developmental Biology*, 92:73–129, 2010.

Z. Ferjentsik, S. Hayashi, J. K. Dale, Y. Bessho, A. Herreman, B. De Strooper, G. del Monte, J. L. de la Pompa, and M. Maroto. Notch is a critical component of the mouse somitogenesis oscillator and is essential for the formation of the somites. *PLoS Genetics*, 5(9):e1000662, 2009.

Alexander George Fletcher. *Aspects of tumour modelling from the subcellular to the tissue scale*. PhD thesis, Oxford University, 2010.

S. Gibb, M. Maroto, and J. K. Dale. The segmentation clock mechanism moves up a notch. *Trends in Cell Biology*, 20(10):593–600, 2010.

K. Hori, A. Sen, and S. Artavanis-Tsakonas. Notch signaling at a glance. *Journal of Cell Science*, 126(10):2135–2140, 2013.

Kazuki Horikawa, Kana Ishimatsu, Eiichi Yoshimoto, Shigeru Kondo, and Hiroyuki Takeda. Noise-resistant and synchronized oscillation of the segmentation clock. *Nature*, 441(7094):719, 2006.

A. Hubaud and O. Pourquié. Signalling dynamics in vertebrate segmentation. *Nature Reviews Molecular Cell Biology*, 15(11):709, 2014.

K. Ishimatsu, T. W. Hiscock, Z. M. Collins, D. W. K. Sari, K. Lischer, D. L. Richmond, Y. Bessho, T. Matsui, and S. G. Megason. Size-reduced embryos reveal a gradient scaling based mechanism for zebrafish somite formation. *Development*, 145(11), 2018.

Y.-J. Jiang, B. L. Aerne, L. Smithers, C. Haddon, D. Ish-Horowicz, and J. Lewis. Notch signalling and the synchronization of the somite segmentation clock. *Nature*, 408(6811):475, 2000.

A. J. Krol, D. Roellig, M.-L. Dequéant, O. Tassy, E. Glynn, G. Hattem, A. Mushegian, A. C. Oates, and O. Pourquié. Evolutionary plasticity of segmentation clock networks. *Development*, 138(13):2783–2792, 2011.

V. M. Lauschke, C. D Tsiairis, P. François, and A. Aulehla. Scaling of embryonic patterning based on phase-gradient encoding. *Nature*, 493(7430):101, 2013.

Y. Masamizu, T. Ohtsuka, Y. Takashima, H. Nagahara, Y. Takenaka, K. Yoshikawa, H. Okamura, and R. Kageyama. Real-time imaging of the somite segmentation clock: revelation of unstable oscillators in the individual presomitic mesoderm cells. *Proceedings of the National Academy of Sciences*, 103(5):1313–1318, 2006.

L. G. Morelli, S. Ares, L. Herrgen, C. Schröter, F. Jülicher, and A. C. Oates. Delayed coupling theory of vertebrate segmentation. *HFSP Journal*, 3(1):55–66, 2009.

P. J. Murray, P. K. Maini, and R. E. Baker. The clock and wavefront model revisited. *Journal of Theoretical Biology*, 283(1):227–238, 2011.

P. J Murray, P. K. Maini, and R. E. Baker. Modelling delta-notch perturbations during zebrafish somitogenesis. *Developmental Biology*, 373(2):407–421, 2013.

Y. Okubo, T. Sugawara, N. Abe-Koduka, J. Kanno, A. Kimura, and Y. Saga. Lfng regulates the synchronized oscillation of the mouse segmentation clock via trans-repression of notch signalling. *Nature Communications*, 3:1141, 2012.

J. Pitt-Francis, P. Pathmanathan, M. O. Bernabeu, R. A. Bordas, J. A. Cooper, A.G. Fletcher, G.R. Mirams, P. J. Murray, J. M. Osborne, A. Walter, S.J. Chapman, A. Garny, I.M.M. van Leeuwen, P.K. Maini, B. Rodrguez, S.L. Waters, J.P. Whiteley, H.M. Byrne, and D.J. Gavaghan. Chaste: A test-driven approach to software development for biological modelling. *Computer Physics Communications*, 180(12):2452–2471, 2009.

O. Pourquié. Somite formation in the chicken embryo. *The International Journal of Developmental Biology*, 62(1-2-3):57–62, 2018.

D. R. Primmett, C. D. Stern, and R. J. Keynes. Heat shock causes repeated segmental anomalies in the chick embryo. *Development*, 104(2):331–339, 1988.

D. R. Primmett, W. E. Norris, G. J. Carlson, R. J. Keynes, and C. D. Stern. Periodic segmental anomalies induced by heat shock in the chick embryo are associated with the cell cycle. *Development*, 105(1):119–130, 1989.

D. Soroldoni, D. J. Jörg, L. G. Morelli, D. L. Richmond, J. Schindelin, F. Jülicher, and A. C. Oates. A doppler effect in embryonic pattern formation. *Science*, 345 (6193):222–225, 2014.

G. Wiedermann, R. A. Bone, J. C. Silva, M. Bjorklund, P. J. Murray, and J. K. Dale. A balance of positive and negative regulators determines the pace of the segmentation clock. *eLife*, 4:e05842, 2015.

A Appendix

Supplementary Movie 1

A movie illustrating spatio-temporal dynamics presented in Figure 3. Left - $\sin(\theta)$ is plotted against x and y. Middle - Natural oscillator frequency is plotted against x, y and t. Right - Cell cycle phase is plotted against x, y and t (0 - Differentiated cell, 1 - G_0/G_1, 2-S, 3 - G_2, 4-M.)

Supplementary Movie 2

A movie illustrating spatio-temporal dynamics presented in Figure 4. Left - $\sin(\theta)$ is plotted against x and y. Middle - Natural oscillator frequency is plotted against x, y and t. Right - Cell cycle phase is plotted against x, y and t (0 - Differentiated cell, 1 - G_0/G_1, 2-S, 3 - G_2, 4-M.)

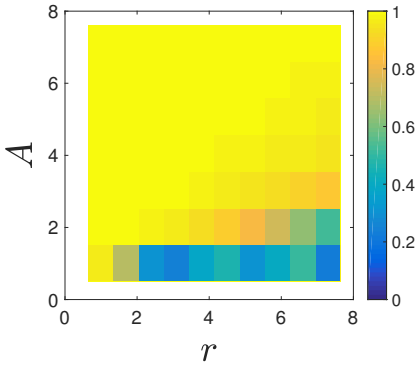

Figure 8: The order parameter is plotted against coupling strength and acceleration factor.

Supplementary Movie 3

A movie illustrating spatio-temporal dynamics presented in Figure 5. Left - $\sin(\theta)$ is plotted against x and y. Middle - Natural oscillator frequency is plotted against x, y and t. Right - Cell cycle phase is plotted against x, y and t (0 - Differentiated cell, 1 - G_0/G_1, 2-S, 3 - G_2, 4-M.)

Supplementary Movie 4

A movie illustrating spatio-temporal dynamics presented in Figure 6. Left - $\sin(\theta)$ is plotted against x and y. Middle - Natural oscillator frequency is plotted against x, y and t. Right - Cell cycle phase is plotted against x, y and t (0 - Differentiated cell, 1 - G_0/G_1, 2-S, 3 - G_2, 4-M.)

Supplementary Movie 5

A movie illustrating spatio-temporal dynamics presented in Figure 7. Left - $\sin(\theta)$ is plotted against x and y. Middle - Natural oscillator frequency is plotted against x, y and t. Right - Cell cycle phase is plotted against x, y and t (0 - Differentiated cell, 1 - G_0/G_1, 2-S, 3 - G_2, 4-M.)

B Phase diagram